analytical chemistry

Subscriber access provided by UNIV OF LOUISIANA

Article

A rationally optimized fluorescent probe for imaging mitochondrial SO2 in HeLa cells and zebrafish

Guang Chen, Wei Zhou, Chenyang Zhao, Yuxia Liu, Tao Chen, Yulin Li, and Bo Tang

Anal. Chem., **Just Accepted Manuscript** • DOI: 10.1021/acs.analchem.8b01505 • Publication Date (Web): 09 Oct 2018

Downloaded from http://pubs.acs.org on October 9, 2018

Just Accepted

"Just Accepted" manuscripts have been peer-reviewed and accepted for publication. They are posted online prior to technical editing, formatting for publication and author proofing. The American Chemical Society provides "Just Accepted" as a service to the research community to expedite the dissemination of scientific material as soon as possible after acceptance. "Just Accepted" manuscripts appear in full in PDF format accompanied by an HTML abstract. "Just Accepted" manuscripts have been fully peer reviewed, but should not be considered the official version of record. They are citable by the Digital Object Identifier (DOI®). "Just Accepted" is an optional service offered to authors. Therefore, the "Just Accepted" Web site may not include all articles that will be published in the journal. After a manuscript is technically edited and formatted, it will be removed from the "Just Accepted" Web site and published as an ASAP article. Note that technical editing may introduce minor changes to the manuscript text and/or graphics which could affect content, and all legal disclaimers and ethical guidelines that apply to the journal pertain. ACS cannot be held responsible for errors or consequences arising from the use of information contained in these "Just Accepted" manuscripts.

ACS Publications

is published by the American Chemical Society. 1155 Sixteenth Street N.W., Washington, DC 20036

Published by American Chemical Society. Copyright © American Chemical Society. However, no copyright claim is made to original U.S. Government works, or works produced by employees of any Commonwealth realm Crown government in the course of their duties.

A rationally optimized fluorescent probe for imaging mitochondrial SO_2 in HeLa cells and zebrafish

Guang Chen[a, b], Wei Zhou[a], Chenyang Zhao[a], Yuxia Liu*[a,b], Tao Chen[c], Yulin Li[c] and Bo Tang*[b]

[a.] The Key Laboratory of Life-Organic Analysis; Key Laboratory of Pharmaceutical Intermediates and Analysis of Natural Medicine, College of Chemistry and Chemical Engineering, Qufu Normal University, Qufu 273165, China.

[b.] College of Chemistry, Chemical Engineering and Materials Science, Collaborative Innovation Center of Functionalized Probes for Chemical Imaging in Universities of Shandong, Key Laboratory of Molecular and Nano Probes, Ministry of Education, Institute of Molecular and Nano Science, Shandong Normal University, Jinan 250014, P. R. China.

*E-mail: tangb@sdnu.edu.cn; Tel.: +86 0531-86180010. Fax: +86 0531-86180017; *E-mail: liuyuxia2008@163.com.

[c.] Key Laboratory of Tibetan Medicine Research & Qinghai Key Laboratory of Qinghai-Tibet Plateau Biological Resources, Northwest Institute of Plateau Biology, Chinese Academy of Science, Xining 810001, Qinghai, PR China.

ABSTRACT: Organism has built up immunologic system, where mitochondrial SO_2 plays the conflicting roles in regulating cell apoptosis. However, no exploration on the influence and regulating principle of mitochondrial SO_2 to the specific apoptosis type can be found, which brings about challenge to fluorescent probe. Herein, we optimize the fluorophore and develop a new fluorescent probe FHMI ((E)-4-(3-formyl-4-hydroxystyryl)-1-methylpyridin-1-iumiodide) by equipping an ICT (intramolecular charge transfer) fluorophore HMII ((E)-4-(4-hydroxystyryl)-1-methylpyridin-1-ium iodide) with an aldehyde group that serves as both fluorescence quencher and reporting group. After the optimization, although the non-conjugated electron donor is formed when sensing SO_2, the preset ICT fluorophore HMII is permitted to release the fluorescence at the enlarged wavelength. Comparing with the traditional design, the probe FHMI exhibit obvious enhanced fluorescence with large red shift. FHMI is successfully applied to the mechanistic exploration of the dichotomous effects of mitochondrial SO_2 to cells apoptosis, showing that mitochondrial SO_2 regulates the early apoptosis of HeLa cells via the reduction of mitochondrial membrane potential. FHMI is applied to explore the dichotomous bio-influence of mitochondrial SO_2 to HeLa cells under oxidative stress, visualizing the regulative role of mitochondrial SO_2 in the apoptotic process. For the first time, the mitochondrial SO_2 is visually found to be closely associated with the early apoptosis of HeLa cells. Moreover, FHMI proves to be readily applicable to monitoring endogenous SO_2 in zebrafish. This probe can act as an effective optical tool for exploring SO_2 in bio-specimen.

Mammalian cells are always kept in the oxidative siege where their survival requires an appropriate balance between oxidants and antioxidants. Overproduction of reactive oxygen species (ROS) or the failure in antioxidant defenses against ROS will cause pathogenesis, such as metabolic syndrome[1], DNA damage[2] and even carcinogenesis[3]. Evidence shows that an altered redox status accompanied by the elevated ROS has nearly always been observed in cancer cells, where the redox signaling regulates various transcription factors[4]. As the reflection of oxidative stress, the transcription factors in turn control the expression of anti-apoptosis, proliferation and angiogenesis[5,6]. By virtue of natural evolution, organism has built up immunologic mechanism, through which the antioxidant agents can counter the rising of ROS by suppressing the pathway of oxidative stress[7]. Therefore, exploration of reciprocal relationship between oxidative-stress with the antioxidant capacity is of great significance to organism[8,9].

Sulfur dioxide (SO_2), existing with the form of HSO_3^- in organism, can be produced via the oxidation of sulphur-containing amino acids or the decomposition of sulfinylpyruvate[10]. Increasing studies suggest that SO_2, participates actively in regulating the redox status as an antioxidant against ROS[11-14]. However, SO_2 also possesses the potential oxidative ability[15,16], thus in the complicated bio-environment, SO_2 may act as both the signaling molecule and the oxidative stress-inducer. Therefore, exploring the cross-talk influence of SO_2 with ROS to cells is very significant for further understanding the dichotomous role of SO_2 inside the cell[17]. Mitochondria plays the key roles in metabolic regulation of the innate and adaptive immune responses to cellular damage and stress[18]. With the glutamate, mitochondria can localize the aspartate aminotransferase, catalyzing the reactions of L-cysteine to generate SO_2[19,20]. Given the anti-oxidative role of SO_2, whatever the absolute amount of mitochondrial SO_2, it is likely that the mitochondrial SO_2 may suppress the oxidative stress and retard the progression of cell apoptosis under oxidative stress. Conversely, given the oxidative effect of SO_2, the damaged mitochondria may set in motion a vicious cycle of

cell apoptosis, leading to the increased ROS production which in turn leads to more cell apoptosis[21-23]. Taking into account the conflicting properties of SO_2 together, we reason that in-depth exploring the dichotomous role of mitochondrial SO_2 will provide invaluable information for cellular regulatory mechanisms, promising to promote the development of chemotherapeutic intervention for cancer cells. Unfortunately, no report yet describing the conflicting effects of mitochondrial SO_2 on the apoptotic regulation of cancer cells was found by us. Furthermore, as far as the apoptosis types are concerned, different apoptosis, such as early or late apoptosis, reflect their respective regulating principles. For example, oxidative stress causes the DNA fragmentation that is closely associated with late apoptosis[24,25]. However, no exploration on the influence and regulating principle of mitochondrial SO_2 to the specific apoptosis type can be found. Therefore, the growing interest in mitochondrial SO_2 drives us to focus on these studies.

Though many excellent fluorescent probes for SO_2 have been developed[26-32], no report yet describing the conflicting effects of mitochondrial SO_2 on apoptotic regulation can be found. Moreover, many probes suffer the blue shift due to the non-coplanar addition reaction of SO_2, which was not satisfactory enough for biological imaging. Herein, we conceived a smart ICT probe FHMI by optimize the fluorophore. As illustrated in Scheme 1, first, we designed an ICT fluorophore HMII which exhibited the strong fluorescence at 525 nm. Then, we equipped the aldehyde to the HMII as both the quenching and the weak electron-withdrawing effect, and achieved the probe FHMI. When reacted with SO_2, FHMI exhibited the strong fluorescence at 560 nm. Comparing with the traditional design as shown in FMPI/HTMI, HHMI showed the enhanced fluorescence as well as the 100 nm of read shift. FHMI was used to in-depth explore the bio-effect and the regulating principle of mitochondrial SO_2 on the cells apoptosis. For the first time, the mitochondrial SO_2 was found to be closely related with the early apoptosis of HeLa cells via the reduction of mitochondrial membrane potential with the aid of fluorescence imaging. Under the oxidative stress, the dichotomous influence of mitochondrial SO_2 to HeLa cells was explored. In addition, the developed probe FHMI was applied to the fluorescence imaging of SO_2 in zebrafish, showing its robust applicability.

EXPERIMENTAL SECTION

Synthesis of probe. To the solution of phenol (300 mg, 3.19 mmol) in toluene (20 mL), acetic acid (25 mL) and hexamethylenetetramine (983 mg, 7.03 mmol) were successively added. The orange solution was refluxed until all the starting material was consumed (18 hrs). The mixture was then cooled to room temperature and poured into 6M HCl (30 mL). The product was extracted with ethyl acetate (3 × 20 mL). The combined organic extracts were washed with saturated brine (40 mL) and then dried over Na_2SO_4. The crude product was purified by column chromatography (silica gel, ethyl acetate: hexane = 1:10) to obtain 2,4-diformylphenol (215 mg, 45% yield) as yellow powder. Characterizations: ^{1}H NMR (500 M, d_6-DMSO): 11.55 (s, 1H), 10.00 (s, 1H), 9.94 (s, 1H), 8.14 (d, J = 2.1 Hz, 1H), 8.07 (dd, J = 8.7, 2.1 Hz, 1H), 7.13 (d, J = 8.7 Hz, 1H). m/z calcd for [$^+$H-$C_8H_6O_3$]: 151.06, found: 151.0131. A solution of 4-methylpeidine (4 mL, 2 mmol) in diethyl ether (12 mL) was treated with methyl iodide (1.5 mL, 2.5 mmol). After reaction, the crystalline 1,4-dimethylpyridin-1-ium iodide was isolated. Characterizations: ^{1}H NMR (500 M, d_6-DMSO): δ 9.13 (d, J =6.5, Hz, 1H), 7.87 (d, J =6.0, Hz, 2H), 4.61 (s, 3H), 2.67 (s, 3H). m/z calcd for [$C_7H_{10}N^+$]: 108.08, found: 108.0804. A mixture of 2,4-diformylphenol (10 mg, 0.067 mmol), piperidine (100 μL, 0.133 mmol) and 4-methylpeidine iodoide (31.2 mg, 0.133 mmol) was dissolved in EtOH (10 mL). The mixture was stirred for 30 min at 80 ^{o}C under an N_2 atmosphere to give the compound FHMI as a yellow solid (20 mg, 80% yield). Characterizations for FHMI: ^{1}H NMR (500 MHz, d_6-DMSO): δ= 9.39 (s, 1H), 8.79 (d, J =7.0 Hz, 2H), 8.01 (s, 1H), 7.97 (s, 2H), 7.91 (d, J =6.5 Hz, 1H), 7.80 (d, J =2.0 Hz, 1H), 7.67 (s, 1H), 7.64 (s, 1H), 7.39 (dd, J =2.5, 2.5 Hz, 1H), 6.32(d, J =9.0 Hz, 1H), δ 4.10 (s, 3H). ^{13}C NMR (125.8 MHz, d_6-DMSO): δ= 187.38, 179.58, 155.65, 144.25, 143.01, 121.88, 119.49, 117.37, 46.39. m/z calcd for [$C_{15}H_{14}NO_2^+$]: 240.10, found: 240.2533. The compounds HMII and FMPI were also prepared (Supporting Information).

Visualizing mitochondrial SO_2 on cells apoptosis under oxidative stress. To investigate the dichotomous roles of mitochondrial SO_2, the cross-talk experiments were performed. First, HeLa cells were pretreated with the DMEM (Dulbecco′s modified eagle media) medium containing FHMI (10 μM) for 30 min and the medium containing MTR (Mito-Tracker®Red, 0.08 μM) for 15 min, respectively. Then BTSA (N-benzyl-2,4-dinitrophenylsulfonamide, 200 μM) was added to endogenously generate the SO_2 in absence or presence of NaClO (100 μM). The resultant cells were incubated for 3 h. As the control experiment, HeLa cells pretreated with probe FHMI (10 μM) and MTR (0.08 μM) were directly stimulated by the media containing NaClO (100 μM) for 3 h. The whole process was followed by confocal laser scanning microscope (Japan Olympus Co., Ltd) with an objective lens (×10) and the flow cytometry (ACEA NovoCyte, Hangzhou, China) to report the homeostasis of mitochondrial SO_2 and the cellular apoptosis rate. Annexin V-FITC (fluorescein isothiocyanate) and PI (propidium iodide) was used to indicate the different population of cells in the apoptosis analysis. To follow the change of mitochondrial membrane potential, HeLa cells was incubated with JC-1 staining working solution (50 μL JC-1 in 8000 μL H_2O and 2000 μL staining buffer) in absence or presence of BTSA (200 μM) for 3 h. The resultant cells were analyzed with the confocal laser scanning microscope with excitation wavelengths set as 515 and 488 nm and collection wavelengths set as 600−700 nm and 500-600, respectively.

Fluorescence imaging in zebrafish. Zebrafishes were provided by HuanTe biological corporation (Hangzhou,

China). Zebrafishes were incubated in E3 media (15 mM NaCl, 0.5 mM KCl, 1 mM $MgSO_4$, 1 mM $CaCl_2$, 0.15 mM KH_2PO_4, 0.05 mM Na_2HPO_4 and 0.7 mM $NaHCO_3$; pH 7.5) containing 10 μM FHMI probe at 28 °C for 1 h, and then, the residual probe was washed by the E3 media. To image the HSO_3^-, zebrafish larvae (three-days) were put into a 50 mm Petri dish filled with E3 media containing BTSA for 1~5 h. Fluorescence imaging was subsequently carried out with a confocal laser scanning microscope (Japan Olympus Co., Ltd) with an objective lens (×10). The excitation wavelengths were 515 nm and 488 nm, and collection windows were at 600−700 nm and 500-600 nm, respectively. All animal experiments were performed in full compliance with international ethical guidelines.

RESULTS AND DISCUSSION

Optimizing the design for probe FHMI. Our inspiration came from the optical properties of FMPI (Scheme 1A (b)). We found that the two acceptors co-planar in FMPI led to the weak response at 450 nm. This phenomena indicated that, without a donor, the ICT suffered fluorescence quenching when SO_2 had a non-coplanar addition reaction with probe. Thus, we thought about to improve the fluorescence intensity by equipping an electron donor to the Π system. Accordingly, we synthesized HMII following Scheme 1A (a) and investigated the contribution of a donor to fluorescence enhancement. As expected, HMII exhibited both the strong fluorescence intensity (Ø=0.66) and the red shift of emission (75 nm) relative to FMPI (Figure 1A). Optical comparison of HMII and FMPI provided us the enlightenment that if the electron-withdrawing quencher could be constructed, the probe would be in the fluorescence off state. To put this conception into action, we performed Scheme 1A (c) and obtained probe FHMI. As a result, FHMI exhibited weak fluorescence (Ø=0.02), indicating that aldehyde effectively quenched the fluorescence. Upon the addition reaction by HSO_3^-, FHMI was transformed to the product HHMI (Ø=0.38) which exhibited the obviously enhanced fluorescence. Moreover, comparing with FMPI, probe FHMI exhibited large red shift (100 nm) in emission, indicating that aldehyde served as not only the fluorescence quencher but also the weak electron-withdrawing group. To confirm this point, we performed series of investigation. ^{1}HNMR titration of FHMI (Figure S2) indicated, upon addition of $NaHSO_3$, the peak of aldehyde H at 9.39 ppm disappeared and a new peak at 6.51 ppm rose up, demonstrating the transformation of aldehyde-H to quaternary carbon-H. Meanwhile, the appearance of peaks at 3.63 ppm indicated the formation of hydroxyl H in this quaternary carbon. Moreover, the appearance of peaks at 10.15 ppm displayed the sulfonic H in this quaternary carbon. These results confirmed that probe underwent a nucleophilic addition reaction with analyte. To validate the non-coplanar structure and the electronic behavior, we calculated the molecular structure with density functional theory (DFT)[33-36]. As displayed in Scheme 2B, the molecule FHMI had a large planar conjugated structure in which the hydroxyl oxygen (donor), the ketonic oxygen (acceptor-2) as well as the positive nitrogen (acceptor-1) were included. When sensing HSO_3^-, as illustrated in Scheme 2B, FHMI was transformed to the product HHMI, forming a saturated hydroxyl oxygen. Clearly, this oxygen

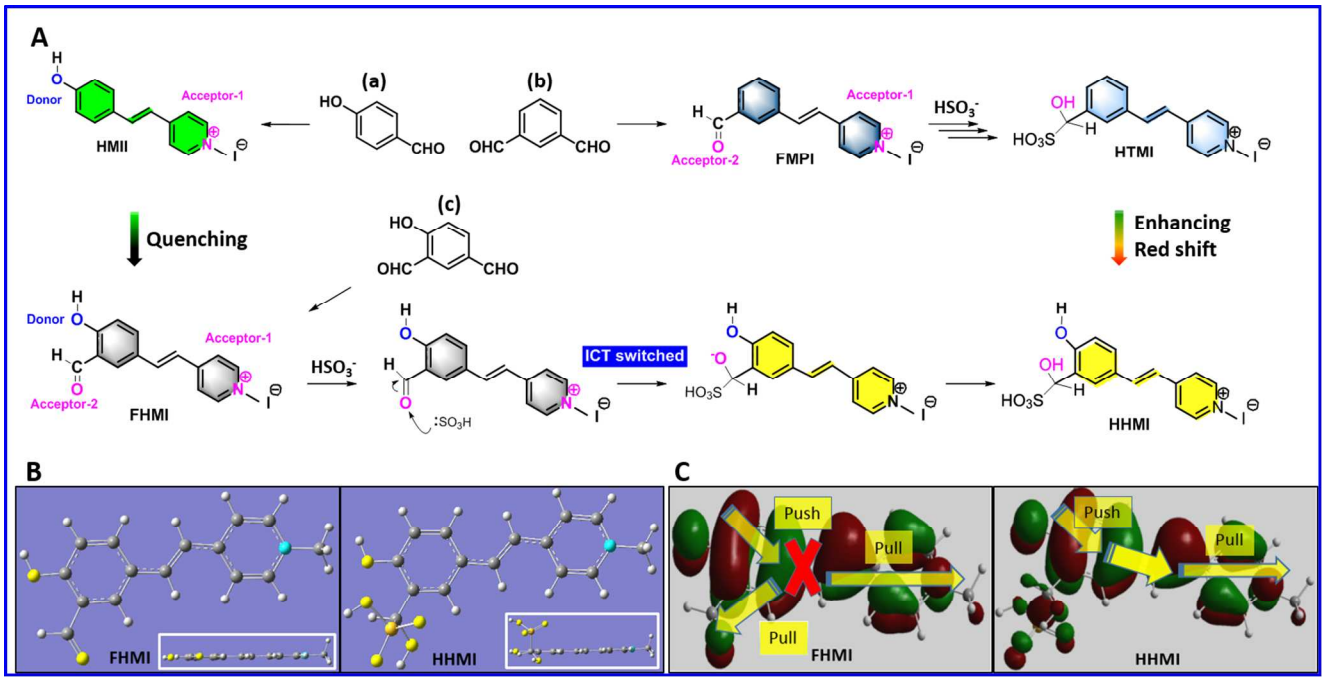

Scheme 1. A) Optimization of probe design; B) Theoretic calculation for the optimized structures of FHMI and HHMI; C): Dissection of the HOMO molecular orbital for illustrating the switch of electron push-pull. Green and red shapes are corresponding to the different phases of the molecular wave functions for HOMO orbitals.

was no more co-planar with the large conjugated system and therefore was no more competitive with the positive nitrogen (acceptor-1) in electron-withdrawing. To further confirm this phenomena, we dissected the molecular orbitals for both FHMI and HHMI. As shown in Scheme 2C, molecular orbital of ketonic group in FHMI displayed the continuously conjugated Π orbital with hydroxyl oxygen (electron donor) and positive nitrogen (electron acceptor). In contrast, the molecular orbitals of HSO_3^--added ketonic group in HHMI was fragmented and no more included in the Π orbital. Consequently, above optical properties, experimental results and theoretical calculation demonstrated that the probe FHMI was rationally constructed after an optimization of designing.

Optical properties of probe FHMI. Time-dependent fluorescence (Figure S6) of FHMI versus HSO_3^- showed that maximal response could be achieved within 60 s. This rapid response could meet the requirement of in-situ monitoring. As the time progressed, the fluorescence exhibited a steady signal, indicating the satisfactory photostability. The pH-dependent fluorescent response of FHMI to HSO_3^- was investigated. As shown in Figure S7, the probe FHMI itself did not respond to the tested pH values (4.80~10.34). In presence of $NaHSO_3$, the pKa was estimated as 7.10.

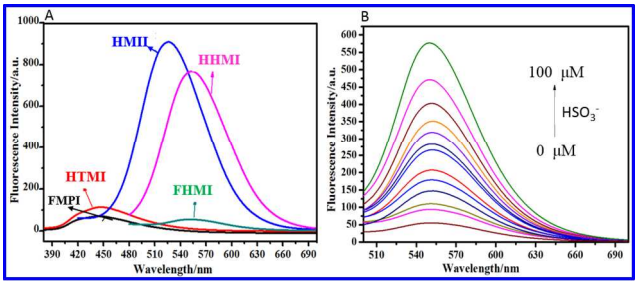

Figure 1. A) Fluorescence properties for the synthesized compounds (FHMI (10 μM), HMII (10 μM), FMPI (10 μM), HHMI(FHMI (10 μM)+ HSO_3^- (300 μM)) and HTMI (FMPI (10 μM)+ HSO_3^- (300 μM))) (FHMI and HHMI: λex=460 nm; HMII: λex=400 nm; FMPI and HTMI: λex=360 nm); B) Fluorescence response of probe FHMI (10 μM) to HSO_3^- (0-100 μM) All experiments were performed in DMSO/PBS buffer solution (9/1, v/v, pH = 7.4) at 37 °C.

Though there were the response change during pH of 6.84~7.40, this change was insignificant. Moreover, the mitochondrial pH value was in the range 7.5~8.5[37,38]. Thus, the heterogeneous pH in mitochondria would not influence the working of probe FHMI. Temperature-dependent fluorescence was tested (Figure S8), showing that the highest response of FHMI to HSO_3^- could be achieved at the physiological temperature (37 °C). Therefore, FHMI exhibited the potential applicability for biological sample. Before the intracellular application, the selectivity of FHMI to HSO_3^- against other possible interference was tested (Figure S12). Relative fluorescence intensity showed that excessive anions, metal ions and RSS, resulted in insignificant interference. Amino acids were investigated to evaluate whether the amino group would cause interferences through the reaction with aldehyde group of this probe. Results in Figure S12 showed that amino acids caused insignificant interference. Thus, probe FHMI could selectively report SO_2 without being interfered by biologically relevant compounds. In addition, we established linear response of FHMI to HSO_3^- (10-100 μM) (Figure S11) and obtained detection limit of 13.1 nM, which was almost the lowest among the reported SO_2 probes[26-31,39,40]. Therefore, the designed probe FHMI was competent in detecting HSO_3^- in biological samples.

Intracellular properties of FHMI. Dynamic fluorescence imaging (Figure S9) indicated that FHMI could rapidly respond to intracellular HSO_3^-. Fluorescence intensity remained almost unchanged for 300 min, indicating the satisfactory photostability. Before cells analysis, cytotoxicity of FHMI was evaluated by MTT assay (Supporting Information). Figure S13 showed that more than 94% cells remained alive when 10 μM FHMI probe was added for 24 h, demonstrating the low toxicity of FHMI. Since, probe FHMI was designed with a positive group, we speculated that this probe would accumulate in the mitochondria. Thus we carried out the co-staining experiments in HeLa cells

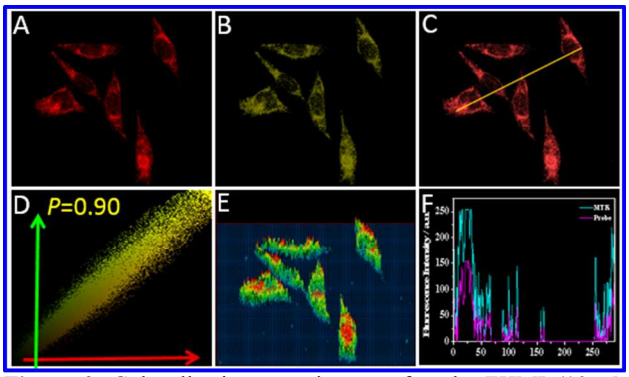

Figure 2. Colocalization experiments of probe FHMI (10 μM) with MitoTracker Red (MTR) (0.08 μM) in HeLa cells. A): MTR; B): FHMI in presence of $NaHCO_3$; C): Merged images of A) and B); D) Colocalization-correlation between red and yellow channels in C) (*P* is the Pearson's co-localization coefficient); E) 3D perspective observation of C). F) Pixel correlation across line in C). Scale bar: 20 μm.

using FHMI with MitoTracker Red (MTR). After being incubated with 10 μM FHMI for 30 min, the HeLa cells were stained with 0.08 μM MTR for 15 min at 37 °C. Figure 2 showed the fluorescence image of HeLa cells with good morphology after co-staining. As illustrated in Figure 2a~b, the mitochondria profiles for MTR and probe FHMI were obtained in two channels. The correlation was estimated with the dependency of fluorescence pixels (Figure 2c, 2f), showing the good correlation between the two group pixels. Pearson's co-localization coefficient was determined to be 0.90, indicating that FHMI predominantly accumulated in mitochondria of living cells. Therefore,

probe FHMI could localize in mitochondria, the main organelle for endogenously generating SO_2 in vivo. To investigate the response of this probe toward intracellular HSO_3^-, we incubated HeLa cells with FHMI (10 μM) and MTR (0.08 μM) in presence of different levels of HSO_3^- (Figure 3), in which, MTR served as both the reference and the control for recording the fluorescence from the site where FHMI and MTR co-localized. As can be seen from Figure 3, the yellow channel showed enhanced fluorescence with the increase of HSO_3^-. The pseudocolored ratio images visualized the increased ratio of I_{probe}/I_{MTR} (0.55-9.21). These results indicated that the developed probe FHMI was suitable for monitoring the mitochondrial HSO_3^-.

Exploring bio-influence of mitochondrial SO_2 to cells apoptosis. SO_2 can be endogenously generated from the sulphur-containing amino acids. Generally, SO_2 exerts the reducing property, serving as an antioxidant to eliminate the excessive ROS[41,42] or as a therapeutic prodrug[43]. While, SO_2 also holds the oxidative potential to cause the injury to cell and tissue[44,45]. Therefore, the reciprocal relationship between oxidative-stress with the anti-oxidative stress is of great significance to organism. In the following experiments, we monitored the mitochondrial SO_2 during cell apoptosis, so that to explore the apoptotic and/or anti-apoptotic effect of mitochondrial SO_2 on cancer cells. HeLa cells were first pretreated by FHMI (10 μM) and MTR (0.08 μM) as the control group. The control cells were then treated with the SO_2 donor BTSA (100 μM) for 3 h in absence or presence of NaClO (100 μM). Besides, the control cells were incubated directly with NaClO (100 μM) for 3 h. As shown in Figure 4 A-1, cells showed mainly the fluorescence in red channel but the negligible fluorescence in yellow channel, indicating the quite low level of mitochondrial SO_2 in the normal cells. Under this condition, we found 97.70% of cells were viable, 1.97% of cells were necrotic, and the apoptotic cells were negligible (Figure 4 B-1; C-1). Stimulation by BTSA would trigger the burst of mitochondrial SO_2. As expected, the obvious yellow emission and the increased ratio of I_{probe}/I_{MTR} were found in Figure 4 A-2, indicating the elevated level of mitochondrial SO_2. Correspondingly, the apoptosis rate was obviously increased (10.04(early)+13.93% (late)), implying the injurious influence of SO_2 to cells.

Since the early apoptosis was always accompanied by the disruption of inner mitochondrial membrane potential[46], we hypothesized that the excessive mitochondrial SO_2 cont ributed to the variation of inner mitochondrial membrane potential (MMP) thereby causing the upregulated early apoptosis[47,48]. To confirm this point, we investigated the MMP by incubating the group 1 and 2 with JC-1 (50 μL JC-1 in 8000 μL H_2O and 2000 μL staining buffer) in absence (left) or presence (right) of BTSA (100 μM) for 3 h (Figure S14). We observed the green fluorescence in group 2 whereas the red fluorescence in group 1. This result confirmed that MMP was reduced in presence of SO_2, which, together with the above findings, justified that the upregulated early apoptosis was associated with the mitochondrial SO_2. To the best of our knowledge, this is the first time that the early apoptosis caused by mitochondrial SO_2 was explored with fluorescence imaging. To perform the further investigation of this phenomena, we imposed artificial intervention of late apoptosis to cells. NaClO could induce the late apoptosis[49], and thus was added before the subsequent addition of BTSA. Figure 4 C-3 showed the remarkable late apoptosis, demonstrating that ClO^- specifically caused the elevated level of late apoptotic cells rather than early apoptotic cells[49]. As a result, the rate of early apoptosis was significantly reduced in contrast to group 2 and correspondingly, the rather weak emission in yellow channel (Figure 4 A-3) was observed. Clearly, the up-regulated late apoptosis and the down-regulated early apoptosis as well as the decreased mitochondrial SO_2 demonstrated the association of early apoptosis with mitochondrial SO_2. Thus, with the aid of FHMI, the injurious effect of mitochondrial SO_2 to cells was visually demonstrated.

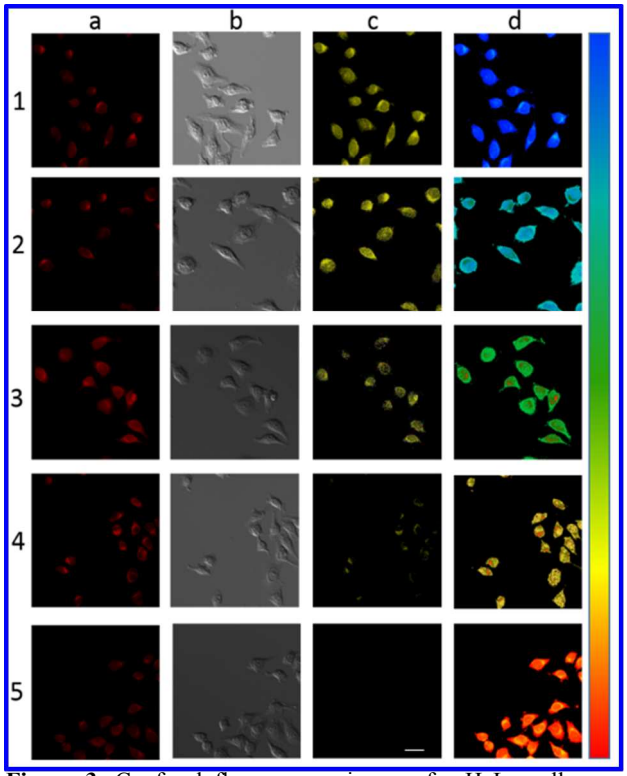

Figure 3. Confocal fluorescence images for HeLa cells pretreated with probe FHMI (10 μM) with addition of different levels of HSO_3^- (1: 80 μM, 2: 60 μM, 3: 40 μM, 4: 20 μM, 5: 0 μM) for 30 min. a): the red channel for MitoTracker Red (0.08 μM); b): the bright field; c) the yellow channel for FHMI; d): the pseudo color images for fluorescence ratio of FHMI with MTR. The color band represented the ratios (I_{probe} /I_{MTR}: 1) 9.21; 2) 7.10; 3) 4.82; 4) 1.79; 5) 0.55.). Scale bar: 20 μm.

Since, SO_2 might play the dichotomous roles in the transduction of the apoptotic and anti-apoptotic signals with its oxidizing and anti-oxidizing properties[50], we were inspired to explore the other effect of SO_2 on regulating the apoptotic system. Apoptotic analysis induced directly by

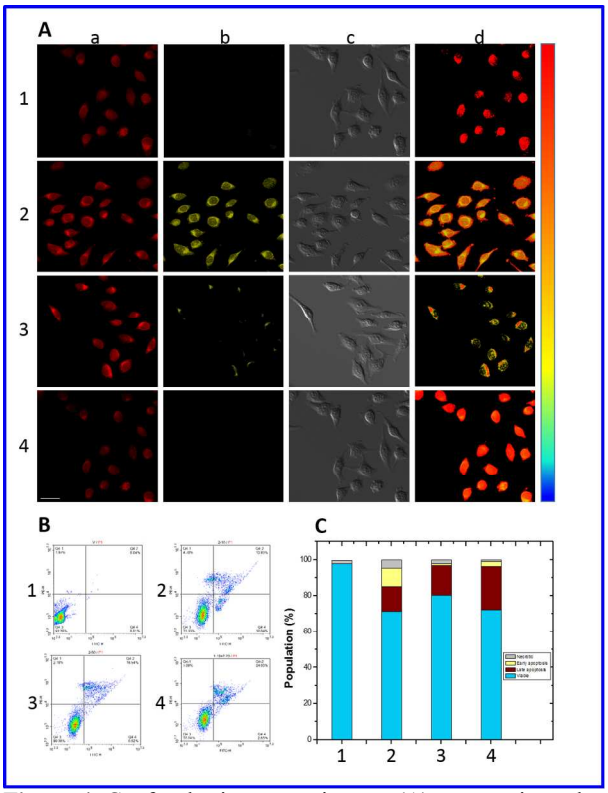

Figure 4. Confocal microscopy images (A), apoptosis analysis (B) and apoptotic population (C). HeLa cells were incubated respectively with probe FHMI (10 μM) for 30 min and then MTR (0.08 μM) for 15 min, to obtain the control group (A-1), and then incubated with BTSA (100 μM) for 3 h in absence (A-2) or presence (A-3) of NaClO (100 μM). To perform comparison, HeLa cells in control group were incubated with the media consisting of NaClO (100 μM) for 3h (A-4). The confocal fluorescence images were collected, including a: the red channel (for I_{MTR}), b: the yellow channel (for I_{probe}), c: bright field, d: the pseudo colour images for the fluorescence ratio of I_{probe}/I_{MTR}. The colour band represented the ratios (I_{probe}/I_{MTR}: 1) 0.79; 2) 5.12; 3) 2.17; 4) 0.69.). The apoptotic population were obtained with the average means from replicated experiments (n=15) and the representative apoptosis distribution was illustrated in C, where 1~4 referred to the four groups of cells. The statistical analysis for apoptosis experiments were performed with Student's t-test: *P <0.05. Scale bar: 20 μm.

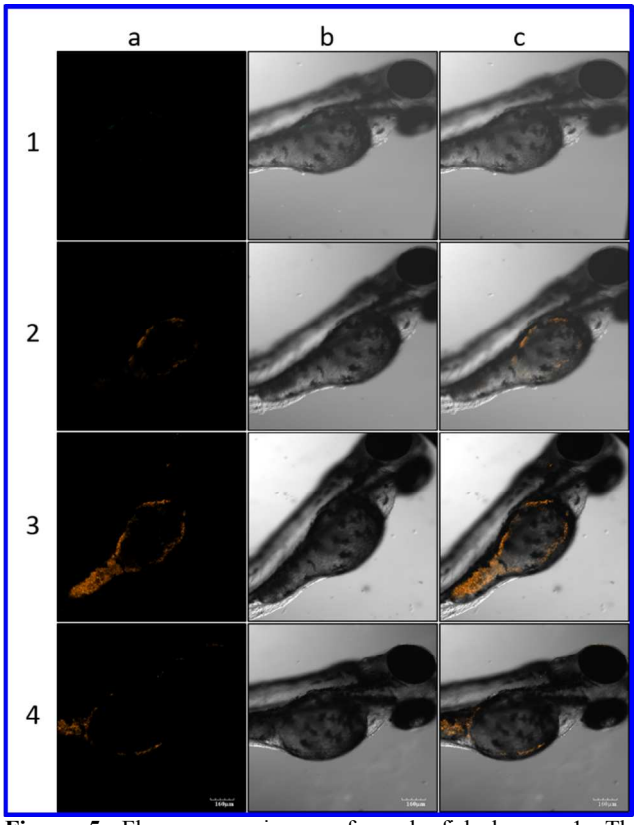

Figure 5. Fluorescence images for zebrafish larvae. 1: The zebrafish was fed with probe FHMI (10 μM) in E3 media for 1 h and was then washed by E3 media; 2: larva pre-treated with procedure 1 was incubated with $NaHSO_3$ (100 μM) for 1 h and was then washed by E3 media; 3: larva pre-treated with procedure 1 was incubated with BTSA (100 μM) for 3 h; 4: larva was incubated with 1 mM N-ethylmaleimide (NEM) and probe FHMI (10 μM) for respective 1.5 h and 1 h, and then was incubated with BTSA for 3 h. Fluorescence images from a to c represented: a): the yellow channel; b): bright-field; c): merged images of a) and b). Scale bar: 20 μm.

NaClO was carried out. As shown in group 4 of Figure 4, almost no fluorescence emission in yellow channel was observed, indicating that NaClO effectively consumed the intracellular SO_2. Meanwhile, as seen from the Figure 4 B-4 and Figure 4 C-4, the late apoptosis rate, was obviously increased comparing with those in group 3. This finding indicated that without the endogenous SO_2, ClO^- lead to more remarkable late apoptosis. To further confirm this result, the late apoptosis was validated by the detection of DNA fragmentation (Figure S15), showing that the increased ClO^- (simultaneously decreased SO_2) caused up-regulated late apoptosis. In return, this result confirmed that in group 3, it was the mitochondrial SO_2 that contributed to the down-regulated late apoptosis. Therefore, the anti-oxidative effect of mitochondrial SO_2 under the oxidative stress was verified. In fact, based on the above experiments, it could be expected that either the SO_2 (induce early apop tosis) or the ClO^- (induce late apoptosis) would cause lower cells viability. As expected, group 3 showed the higher viable rate than both group 2 and group 4, implying that mitochondrial SO_2 might participate the positive modulation of anti-oxidant system to the cells viability under the oxidative stress[42,48,51,52]. Overall, these studies demonstrated that, FHMI was an effective tool to explore the biological role of mitochondrial SO_2.

Imaging endogenous SO_2 in zebrafish. With the satisfactory properties of FHMI, we then tested its applicability in vivo. Since most genes of zebrafish were homologous with those of human, zebrafish was selected as the model for in vivo experiment [53,54]. First, we had the zebrafish incubated in E3 media (15 mM NaCl, 0.5 mM KCl, 1 mM $MgSO_4$, 1 mM $CaCl_2$, 0.15 mM KH_2PO_4, 0.05 mM Na_2HPO_4 and 0.7 mM $NaHCO_3$; pH 7.5) containing 10 μM FHMI for 1 h. As shown in group 1 of Figure 5, almost no fluorescent emission was detected in the yellow

channel, suggesting that the spontaneously generated SO_2 in zebrafish was quite low. Then, the $NaHSO_3$ (100 μM) was added to the medium of group 1 and the incubation was kept for 1 h. As shown in group 2, the fluorescence exhibited obvious enhancement. This result indicated that the elevated HSO_3^- inside the zebrafish triggered the fluorescence of FHMI. To confirm this point, we incubated the zebrafish of group 1 with BTSA (100 μM) for 3 h. Obviously, the enhanced fluorescence intensity was observed in the yellow channel (Figure 5-3), indicating that the amount of SO_2 was elevated by the stimulation of BTSA. For a further confirmation, we carried out the control experiment by adding NEM (N-ethylmaleimide; 1 mM) to the media before the incubation with BTSA. As a result, the Figure 5-4 displayed the rather weak fluorescence intensity. This result indicated that even in presence of the BTSA, the amount of SO_2 in zebrafish was decreased under the inhibitive effect of NEM. Therefore, these experiments demonstrated that the applicability of probe FHMI was robust for various bio-specimen, thus providing the opportunity for the new investigations of whole-organism analysis.

CONCLUSIONS

In summary, we rationally constructed a new mitochondrial SO_2 probe by optimizing the optical properties of the quencher/donor influenced fluorophore. Such a control avoided the potential defects including the fluorescence quenching and emission shortening when sensing SO_2 via the non-planar addition reaction. Comparing with the traditional design, the present probe FHMI exhibit obvious enhanced fluorescence with large red shift. With FHMI, mitochondrial SO_2 was found to be related with the early apoptosis of HeLa cells through reducing the mitochondrial membrane potential. Under the oxidative stress, mitochondrial SO_2 played the regulative role in apoptosis process. Besides, FHMI proved to be applicable in zebrafish for visualizing the endogenously generated SO_2. We therefore envision that this probe can find the extensive application in monitoring mitochondrial SO_2 in biological systems.

ASSOCIATED CONTENT

Supporting Information

The Supporting Information is available free of charge on the ACS Publications website.

Additional detailed information, NMR spectra, mass spectrum, and biological experiments.

AUTHOR INFORMATION

Corresponding Author

* tangb@sdnu.edu.cn; liuyuxia2008@163.com

ACKNOWLEDGMENT

This work was supported by National Natural Science Foundation of China (Nos: 21535004, 91753111, 21390411, 21475074, 21403123), the China Postdoctoral Science Foundation (2017M622254; 2016M600531), the Open Funds of the Shandong Province Key Laboratory of Detection Technology for Tumor Markers (KLDTTM2015-6; KLDTTM2015-9), and the Natural Science Foundation of Shandong Province (ZR201709240033).

REFERENCES

(1) Bonomini, F.; Rodella, L. F.; Rezzani, R. Metabolic Syndrome, Aging and Involvement of Oxidative Stress. *Aging Dis* **2015**, *6*, 109.

(2) Fu, X. Y.; Yang, M. F.; Cao, M. Z.; Li, D. W.; Yang, X. Y.; Sun, J. Y.; Zhang, Z. Y.; Mao, L. L.; Zhang, S.; Wang, F. Z. Strategy to Suppress Oxidative Damage-Induced Neurotoxicity in PC12 Cells by Curcumin: the Role of ROS-Mediated DNA Damage and the MAPK and AKT Pathways. *Mol Neurobiol* **2016**, *53*, 369.

(3) Nathan, C.; Cunninghambussel, A. Beyond oxidative stress: an immunologist's guide to reactive oxygen species. *Nat Rev Immunol* **2013**, *13*, 349.

(4) Trachootham, D.; Alexandre, J.; Huang, P. Targeting cancer cells by ROS-mediated mechanisms: a radical therapeutic approach? *Nat Rev Drug Discov* **2009**, *8*, 579.

(5) Muinelo-Romay, L.; Alonso-Alconada, L.; Alonso-Nocelo, M.; Barbazan, J.; Abal, M. Tumor Invasion and Oxidative Stress: Biomarkers and Therapeutic Strategies. *Curr Mol Med* **2012**, *12*, 746.

(6) Gorrini, C.; Harris, I. S.; Mak, T. W. Modulation of oxidative stress as an anticancer strategy. *Nat Rev Drug Discov* **2013**, *12*, 931.

(7) Schafer, Z. T.; Grassian, A. R.; Song, L.; Jiang, Z.; Gerhart-Hines, Z.; Irie, H. Y.; Gao, S.; Puigserver, P.; Brugge, J. S. Antioxidant and oncogene rescue of metabolic defects caused by loss of matrix attachment. *Nature* **2011**, *461*, 109.

(8) Navarro, J.; Obrador, E.; Carretero, J.; Petschen, I.; Aviñó, J.; Perez, P.; Estrela, J. M. Changes in glutathione status and the antioxidant system in blood and in cancer cells associate with tumour growth in vivo. *Free Radical Bio Med* **1999**, *26*, 410.

(9) Gupte, A.; Mumper, R. J. Elevated copper and oxidative stress in cancer cells as a target for cancer treatment. *Cancer Treat Rev* **2009**, *35*, 32.

(10) Sun, Y.; Liu, J.; Zhang, J.; Yang, T.; Guo, W. Fluorescent probe for biological gas SO_2 derivatives bisulfite and sulfite. *Chem Commun* **2013**, *49*, 2637.

(11) Li, J.; Meng, Z. The role of sulfur dioxide as an endogenous gaseous vasoactive factor in synergy with nitric oxide. *Nitric Oxide* **2009**, *20*, 166.

(12) Wallace, J. L.; Wang, R. Hydrogen sulfide-based therapeutics: exploiting a unique but ubiquitous gasotransmitter. *Nat Rev Drug Discov* **2015**, *14*, 329.

(13) Li, H.; Sun, L.; de Carvalho, E. L.; Li, X.; Lv, X.; Khan, G. J.; Semukunzi, H.; Yuan, S.; Lin, S. DT-13, a saponin monomer of dwarf lilyturf tuber, induces autophagy and potentiates anticancer effect of nutrient deprivation. *Eur J Pharmacol* **2016**, *781*, 164.

(14) Abramovič, H.; Košmerl, T.; Poklar, U. N.; Cigić, B. Contribution of SO_2 to antioxidant potential of white wine. *Food Chem* **2015**, *174*, 147.

(15) Meng, Z. Oxidative damage of sulfur dioxide on various organs of mice: sulfur dioxide is a systemic oxidative damage agent. *Inhal Toxicol* **2003**, *15*, 181.

(16) Kubo, A.; Saji, H.; Tanaka, K.; Kondo, N. Expression of arabidopsis cytosolic ascorbate peroxidase gene in response to ozone or sulfur dioxide. *Plant Mol Biol* **1995**, *29*, 479.

(17) Dou, K.; Fu, Q.; Chen, G.; Yu, F.; Liu, Y.; Cao, Z.; Li, G.; Zhao, X.; Xia, L.; Chen, L.; Wang, H.; You, J. A novel dual-ratiometric-response fluorescent probe for SO_2/ClO^- detection in

cells and in vivo and its application in exploring the dichotomous role of SO_2 under the ClO^- induced oxidative stress. *Biomaterials* **2017**, *133*, 82.
(18) Walker, M. A.; Volpi, S.; Sims, K. B.; Walter, J. E.; Traggiai, E. Powering the Immune System: Mitochondria in Immune Function and Deficiency. *J Immunol Res* **2014**, *2014*, 1.
(19) Masola, B.; Peters, T. J.; Evered, D. F. Transamination pathways influencing l-glutamine and l-glutamate oxidation by rat enterocyte mitochondria and the subcellular localization of l-alanine aminotransferase and l-aspartate aminotransferase. *BBA-Gen Subjects* **1985**, *843*, 137.
(20) Mathew, N. D.; Schlipalius, D. I.; Ebert, P. R. Sulfurous Gases As Biological Messengers and Toxins: Comparative Genetics of Their Metabolism in Model Organisms. *J Toxicol* **2011**, *2011*, 1.
(21) Simon, H. U.; Haj-Yehia, A.; Levi-Schaffer, F. Role of reactive oxygen species (ROS) in apoptosis induction. *Apoptosis* **2000**, *5*, 415.
(22) Finkel, T.; Holbrook, N. J. Oxidants, oxidative stress and the biology of ageing. *Nature* **2000**, *408*, 239.
(23) Dou, K.; Chen, G.; Yu, F.; Liu, Y.; Chen, L.; Cao, Z.; Chen, T.; Li, Y.; You, J. Bright and sensitive ratiometric fluorescent probe enabling endogenous FA imaging and mechanistic exploration of indirect oxidative damage due to FA in various living systems. *Chem Sci* **2017**, *8*, 7851.
(24) Wenzel, U.; Kuntz, S.; Brendel, M. D.; Daniel, H. Dietary Flavone Is a Potent Apoptosis Inducer in Human Colon Carcinoma Cells. *Cancer Res* **2000**, *60*, 3823.
(25) Higuchi, Y. Chromosomal DNA fragmentation in apoptosis and necrosis induced by oxidative stress. *Biochem. Pharmacol.* **2003**, *66*, 1527.
(26) Xu, W.; Teoh, C. L.; Peng, J.; Su, D.; Yuan, L.; Chang, Y.-T. A mitochondria-targeted ratiometric fluorescent probe to monitor endogenously generated sulfur dioxide derivatives in living cells. *Biomaterials* **2015**, *56*, 1.
(27) Liu, Y.; Li, K.; Wu, M. Y.; Liu, Y. H.; Xie, Y. M.; Yu, X. Q. A mitochondria-targeted colorimetric and ratiometric fluorescent probe for biological SO_2 derivatives in living cells. *Chem Commun* **2015**, *51*, 10236.
(28) Yang, J.; Li, K.; Hou, J.-T.; Li, L.-L.; Lu, C.-Y.; Xie, Y.-M.; Wang, X.; Yu, X.-Q. Novel Tumor-Specific and Mitochondria-Targeted near-Infrared-Emission Fluorescent Probe for SO_2 Derivatives in Living Cells. *ACS Sensors* **2016**, *1*, 166.
(29) Li, H.; Yao, Q.; Fan, J.; Hu, C.; Xu, F.; Du, J.; Wang, J.; Peng, X. A Fluorescent Probe for Ratiometric Imaging of SO_2 Derivatives in Mitochondria of Living Cells. *Ind Eng Chem Res* **2016**, *55*, 1477.
(30) Yang, X.; Zhou, Y.; Zhang, X.; Yang, S.; Chen, Y.; Guo, J.; Li, X.; Qing, Z.; Yang, R. A TP-FRET-based two-photon fluorescent probe for ratiometric visualization of endogenous sulfur dioxide derivatives in mitochondria of living cells and tissues. *Chem Commun* **2016**, *52*, 10289.
(31) Wu, W.-L.; Ma, H.-L.; Huang, M.-F.; Miao, J.-Y.; Zhao, B.-X. Mitochondria-targeted ratiometric fluorescent probe based on FRET for bisulfite. *Sensor Actuat B-chem* **2017**, *241*, 239.
(32) Tang, L.; He, P.; Yan, X.; Sun, J.; Zhong, K.; Hou, S.; Bian, Y. A mitochondria-targetable fluorescent probe for ratiometric detection of SO_2 derivatives and its application in live cell imaging. *Sensor Actuat B-chem* **2017**, *247*, 421.
(33) Liu, Y.; Yang, X.; Liu, L.; Wang, H.; Bi, S. Mechanistic insight into water-modulated cycloisomerization of enynyl esters using an Au(I) catalyst. *Dalton Trans* **2015**, *44*, 5354.
(34) Liu, Y.; Chen, G.; Wang, H.; Bi, S.; Zhang, D. Theoretical Investigation of the Controlled Metathesis Reactions of Methylruthenium(II) Complexes with Terminal Acetylenes. *Eur J Inorg Chem* **2014**, *2014*, 2502.
(35) Liu, L.; Liu, Y.; Ling, B.; Bi, S. Mechanistic investigation into Et 3 N C H activation and chemoselectivity by Pd-Catalyzed intramolecular heck reaction of N-Vinylacetamides. *J Organomet Chem* **2017**, *827*, 56.
(36) Liu, Y.; Tang, Y.; Jiang, Y.-Y.; Zhang, X.; Li, P.; Bi, S. Mechanism and Origin of $Et_2Al(OEt)$-Induced Chemoselectivity of Nickel-Catalyzed Three-Component Coupling of One Diketene and Two Alkynes. *ACS Catalysis* **2017**, *7*, 1886.
(37) Sarkar, A. R.; Heo, C. H.; Xu, L.; Lee, H. W.; Si, H. Y.; Byun, J. W.; Kim, H. M. A ratiometric two-photon probe for quantitative imaging of mitochondrial pH values. *Chem Sci* **2016**, *7*, 766.
(38) Chen, G.; Fu, Q.; Yu, F.; Ren, R.; Liu, Y.; Cao, Z.; Li, G.; Zhao, X.-E.; Chen, L.; Wang, H. Wide-acidity-range pH fluorescence probes for evaluation of acidification in mitochondria and digestive tract mucosa. *Anal Chem* **2017**, *89*, 8509.
(39) Li, D.-P.; Wang, Z.-Y.; Cao, X.-J.; Cui, J.; Wang, X.; Cui, H.-Z.; Miao, J.-Y.; Zhao, B.-X. A mitochondria-targeted fluorescent probe for ratiometric detection of endogenous sulfur dioxide derivatives in cancer cells. *Chem Commun* **2016**, *52*, 2760.
(40) Liu, Y.; Li, K.; Xie, K.-X.; Li, L.-L.; Yu, K.-K.; Wang, X.; Yu, X.-Q. A water-soluble and fast-response mitochondria-targeted fluorescent probe for colorimetric and ratiometric sensing of endogenously generated SO_2 derivatives in living cells. *Chem Commun* **2016**, *52*, 3430.
(41) Luo, L.; Chen, S.; Jin, H.; Tang, C.; Du, J. Endogenous generation of sulfur dioxide in rat tissues. *Biochem Biophys Res Commun* **2011**, *415*, 61.
(42) Jin, H. F.; Wang, Y.; Wang, X. B.; Sun, Y.; Tang, C. S.; Du, J. B. Sulfur dioxide preconditioning increases antioxidative capacity in rat with myocardial ischemia reperfusion (I/R) injury. *Nitric Oxide* **2013**, *32*, 56.
(43) Ji, X.; El-labbad, E. M.; Ji, K.; Lasheen, D. S.; Serya, R. A. T.; Abouzid, K. A.; Wang, B. Click and Release: SO_2 Prodrugs with Tunable Release Rates. *Org Lett* **2017**, *19*, 818.
(44) Huang, L. L.; Yang, C.; Zhao, Y.; Xu, X.; Xu, Q.; Li, G. Z.; Cao, J.; Herbert, S. J.; Hao, L. Antioxidant Defenses of Mycorrhizal Fungus Infection Against SO_2-Induced Oxidative Stress in Avena nuda Seedlings. *B Environ Contam Tox* **2008**, *81*, 440.
(45) Arashiro, M.; Lin, Y. H.; Sexton, K. G.; Zhang, Z.; Jaspers, I.; Fry, R. C.; Vizuete, W. G.; Gold, A.; Surratt, J. D. In Vitro Exposure to Isoprene-Derived Secondary Organic Aerosol by Direct Deposition and its Effects on COX-2 and IL-8 Gene Expression. *Atmos Chem Phys* **2016**, *16*, 14079.
(46) Macho, A.; Decaudin, D.; Castedo, M.; Hirsch, T.; Susin, S. A.; Zamzami, N.; Kroemer, G. Chloromethyl-X-Rosamine is an aldehyde-fixable potential-sensitive fluorochrome for the detection of early apoptosis. *Cytometry* **1996**, *25*, 333.
(47) Qin, G.; Wang, J.; Huo, Y.; Yan, H.; Jiang, C.; Zhou, J.; Wang, X.; Sang, N. Sulfur dioxide inhalation stimulated mitochondrial biogenesis in rat brains. *Toxicology* **2012**, *300*, 67.
(48) Wang, X.-B.; Du, J.-B.; Cui, H. Sulfur dioxide, a double-faced molecule in mammals. *Life Sci.* **2014**, *98*, 63.
(49) Carmonagutierrez, D.; Alavianghavanini, A.; Habernig, L.; Bauer, M. A.; Hammer, A.; Rossmann, C.; Zimmermann, A. S.; Ruckenstuhl, C.; Büttner, S.; Eisenberg, T. The cell death protease Kex1p is essential for hypochlorite-induced apoptosis in yeast. *Cell Cycle* **2013**, *12*, 1704.

(50) Qin, G.; Wu, M.; Sang, N. Sulfur dioxide and benzo(a)pyrene trigger apoptotic and anti-apoptotic signals at different post-exposure times in mouse liver. *Chemosphere* **2015**, *139*, 318.
(51) Jin, H.; Du, S.; Zhao, X.; Wei, H.; Wang, Y.; Liang, Y.; Tang, C.; Du, J. Effects of endogenous sulfur dioxide on monocrotaline-induced pulmonary hypertension in rats. *Acta Pharmacol Sin* **2008**, *29*, 1157.
(52) Liang, Y.; Liu, D.; Ochs, T.; Tang, C.; Chen, S.; Zhang, S.; Geng, B.; Jin, H.; Du, J. Endogenous sulfur dioxide protects against isoproterenol-induced myocardial injury and increases myocardial antioxidant capacity in rats. *Lab Invest* **2011**, *91*, 12.
(53) Liu, Y.; Li, D.; Yuan, Z. Photoacoustic Tomography Imaging of the Adult Zebrafish by Using Unfocused and Focused High-Frequency Ultrasound Transducers. *Appl Sci* **2016**, *6*, 392.
(54) Drabsch, Y. Transforming growth factor-β signalling controls human breast cancer metastasis in a zebrafish xenograft model. *Breast Cancer Res* **2013**, *15*, R106.

Table of Contents artwork